Magnetoresistance of semiconductor-metal hybrid structures: The effects of material parameters and contact resistance

Matthias Holz*
I. Institut für Theoretische Physik, Universität Hamburg, Jungiusstrasse 9, 20355 Hamburg, Germany
and Fachbereich Elektrotechnik, Universität der Bundeswehr Hamburg, Holstenhofweg 85, 22043 Hamburg, Germany

Oliver Kronenwerth and Dirk Grundler
Institut für Angewandte Physik und Zentrum für Mikrostrukturforschung, Universität Hamburg, Jungiusstrasse 11, 20355 Hamburg, Germany

(Received 23 October 2002; revised manuscript received 28 January 2003; published 9 May 2003)

We have used the finite element method to study the extraordinary magnetoresistance (EMR) effect of semiconductor-metal hybrid structures in rectangular device geometries. These have recently been found to exhibit intriguing properties interesting for magnetic-field sensors. Current and potential distributions in the devices are calculated in an applied magnetic field. By these means, we investigate the EMR effect, in particular, as a function of material parameters and of the contact resistance ρ_c between the semiconductor and the metal. In our calculations we find that ρ_c should be within a specific operation regime in order to obtain a pronounced magnetoresistance effect. We show that by means of the electron mobility in the semiconductor the voltage and the current sensitivity of a hybrid device can be optimized with respect to an operation field in the 10-mT range.

DOI: 10.1103/PhysRevB.67.195312 PACS number(s): 72.20.My, 72.80.Ey, 72.80.Tm, 85.35.Be

I. INTRODUCTION

Recently, the extraordinary magnetoresistance (EMR) effect has been observed in semiconductor-metal hybrid structures.[1,2] Values for the magnetoresistance $MR=[R(B)-R(0)]/R(0)$ as high as 750 000% have been reported for a magnetic field $B=4$ T at room temperature,[1] where $R(B)$ is the device resistance at magnetic field B. In their pioneering work, Solin *et al.* dealt with EMR devices in a modified van-der-Pauw (vdP) geometry with a circular metallic inclusion in a bulk semiconductor disk.[1,3] It was found by the same group that also in a rectangular geometry the hybrid device showed the EMR effect.[2] Here, a bulk semiconductor was shunted on one side by a metal. This geometry offered even more intriguing technological properties, e.g., if integrated in magnetic-field sensors or read heads.[4,5] Such EMR sensors might be feasible in a very broad temperature regime, ranging from cryogenic[6] up to room temperature.[5,7] Very recently, modulation-doped semiconductor heterostructures have been introduced to the field of the EMR effect. In such hybrid structures, a two-dimensional electron system (2DES) was shunted by a metal film.[4,6] In Ref. 6, it was observed experimentally that in the modulation-doped semiconductor heterostructure a variation of the mobility μ and of the 2DES carrier density N_s significantly changed the EMR effect. So far, InAs-based[6] and InSb-based[4] heterostructures have been involved in EMR studies of hybrid devices. An important difference between these materials is that the latter forms a Schottky barrier if it is in contact with a metal while the former does not. As a result, different specific contact resistances ρ_c might occur. A recent experimental study[8] indicated the decisive role of ρ_c with respect to the magnetoresistance behavior of a hybrid structure. The experimental results on the EMR effect suggest also that there is a complex interplay between material parameters, the contact resistance, and the device geometry. In this paper, we present a theoretical investigation on these subjects. Our results are interesting for, both, basic and applied research on materials and magnetotransport characteristics of hybrid devices.

We have applied the finite element method (FEM) to EMR devices and studied their behavior as a function of material parameters. It has been demonstrated by Moussa *et al.*[9] that the FEM is a powerful tool in studying the magnetotransport in hybrid structures. They modeled the modified vdP geometry[1] and showed a very good agreement between numerical results and, both, experimental data and analytical results. FEM has advantages in so far as it does not require highly symmetric geometries in contrast to analytical calculations.[9] In our study, we address the performance of both types of rectangular devices discussed so far in the literature, i.e., hybrid structures involving a bulk semiconductor[2] (type A) and a 2DES (Ref. 6) (type B). We focus on these two configurations taken from the literature in order to make a comparison between theory and experimental data possible. A summary of the material data and device dimensions for these configurations can be found in Table I. The effect of the mobility, the carrier density, and the contact resistance is evaluated for low magnetic fields up to 100 mT, since it has been argued[5] that this would be the relevant field range for applications of EMR devices as read heads and sensors. The EMR behavior of the devices analyzed here will be discussed in terms of the magnetic-field-dependent resistance $R(B)$ obtained in four-probe configuration, but also in technologically relevant terms like the current sensitivity dR/dB and the voltage sensitivity $1/R\,dR/dB$.

In Sec. II we give a short introduction into the FEM model which we used for our calculations. In Sec. III, we show results of the FEM analysis on the magnetoresistance

TABLE I. Material data and device dimensions of EMR devices from the literature. Type *A* corresponds to the data of Zhou *et al.* (Ref. 2), which were obtained at room temperature, type *B* to the data of Möller *et al.* (Ref. 6), which were obtained at 4.2 K.

Type	Carrier density in the semiconductor	Mobility μ in the semiconductor (T^{-1})	Metal resistivity ρ_m (10^{-8} Ω m)	Device dimensions of semiconductor (μm$\times\mu$m)
A	$n=2.11\times10^{22}$ m^{-3}	4.02	2.2	2140×300
B	$N_s=5.7\times10^{15}$ m^{-2}	14.3	2.2	200×20

of bulk hybrid structures. The model for FEM analysis of 2DES-metal systems is introduced in Sec. IV. The effect of a contact resistance is investigated in Sec. V. In Sec. VI, the dependence of the EMR on the metal conductivity is discussed. The influence of the carrier concentration and mobility in the semiconductor on the EMR effect is reported in Sec. VII. In Sec. VIII, we summarize and discuss the results.

II. FINITE ELEMENT ANALYSIS

The current flow in the semiconductor-metal hybrid structure is given by Ohm's law

$$\mathbf{j}=\boldsymbol{\sigma}\mathbf{E}, \tag{1}$$

where **j** (current density), $\boldsymbol{\sigma}$ (conductivity matrix), and **E** (electric field) are local quantities. We restrict our analysis to two dimensions described by the Cartesian coordinates *x*, *y* and magnetic fields that are perpendicular to the *x*-*y* plane. This procedure requires the existence of a symmetry of the device parallel to the magnetic field direction so that Eq. (1) can be separated into an *x*-*y* and a *z* contribution. This symmetry is present in a bulk semiconductor-metal hybrid structure. The conductivity $\boldsymbol{\sigma}$ depends both on material parameters and magnetic field by

$$\boldsymbol{\sigma}(\beta)=\frac{\sigma_0}{1+\beta^2}\begin{pmatrix}1 & -\beta\\ \beta & 1\end{pmatrix} \tag{2}$$

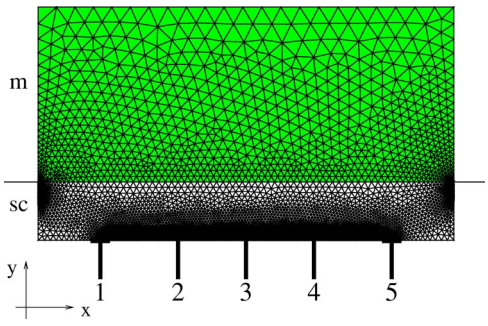

FIG. 1. A mesh generated for a rectangular hybrid structure of type *A* (top view), including current leads and voltage probes. It contains over 10 000 nodes and more than 20 000 triangular elements. The semiconductor (sc) is in the lower, the metal (m) in the upper part of the figure. The mesh was refined in the proximity of the current leads and voltage probes as well as the edges of the semiconductor-metal interface, in order to account for the formation of hot spots as described in the text.

with dimensionless field

$$\beta=\mu B. \tag{3}$$

The Drude conductivity at $B=0$ T is given by

$$\sigma_0=ne\mu, \tag{4}$$

where n is the carrier density and μ is the mobility of the carriers. By means of the continuity equation, for the steady state, we obtain

$$\boldsymbol{\nabla}\cdot[\boldsymbol{\sigma}\boldsymbol{\nabla}V(x,y)]=0 \tag{5}$$

for the electrical potential *V*. In order to apply the FEM, Eq. (5) is rewritten in the form of a variational principle, as described, e.g., in the publication by Moussa *et al.*[9]

Solutions of Eq. (5) are uniquely fixed only if a proper system of boundary conditions is imposed. At the current leads, the current densities perpendicular to the device boundary are fixed, which give rise to the Neumann boundary conditions. This is, however, not sufficient to uniquely determine a solution of Eq. (5). In order to do so, we additionally impose a Dirichlet condition at a certain point of the system, thereby fixing a common electrical ground. For the mesh, we used triangular elements with linear interpolation functions. In order to obtain suitable meshes for the FEM, we used the software EasyMesh[10] and modified it for larger structures. For illustration, a typical mesh, generated for a rectangular hybrid structure, is displayed in Fig. 1. Probes are schematically shown at the bottom of the drawing and are labeled by 1 to 5. The probes labeled by 2, 3, and 4 are used as voltage probes, while the labels 1 and 5 denote the current leads. The mesh is very fine in the proximity of the probes and current leads and at the edges of the semiconductor-metal interface in order to account for the rapidly changing potential in these regions.

For evaluating the potentials, we used pointlike probes in our FEM analysis. To a good approximation, the obtained value could be regarded as the averaged potential if a wider probe was used.

III. MAGNETORESISTANCE OF A BULK SEMICONDUCTOR-METAL HYBRID STRUCTURE

Applying the finite element method to a hybrid structure, we are foremost interested in the magnetic-field-dependent potential distribution $V(\mathbf{r})$. The resistance R can then be defined by

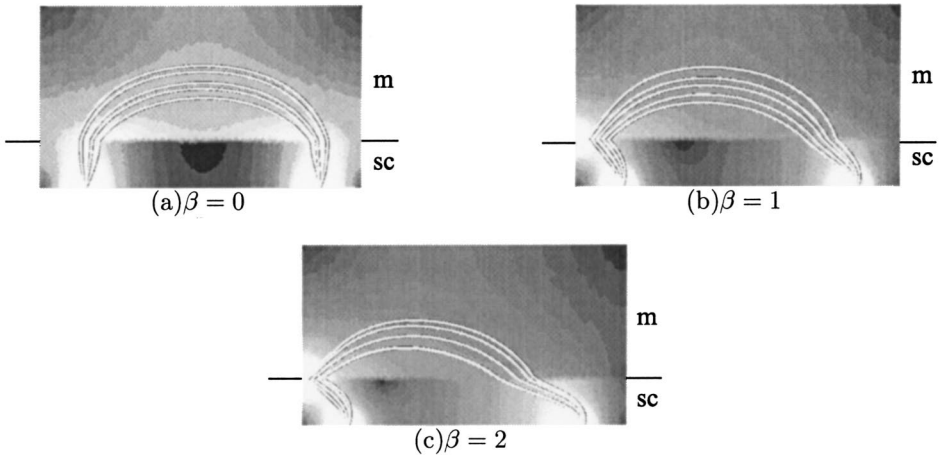

FIG. 2. Current distribution for the device depicted in Fig. 1 (type A) for different magnetic fields. The metal is denoted by m, the semiconductor is by sc. The gray-scaled plot shows the local current density (bright colors correspond to high densities, dark colors to low densities). The bright lines illustrate the current flow starting from equidistant points in the left current lead. The three figures correspond to $B=0$ T, $B=250$ mT, and $B=500$ mT, respectively. At $\beta=2$, current lines get very close on the left-hand side of the semiconductor-metal interface.

$$R(\mathbf{r}_1,\mathbf{r}_2)=\left|\frac{U(\mathbf{r}_1,\mathbf{r}_2)}{I}\right|=\left|\frac{V(\mathbf{r}_1)-V(\mathbf{r}_2)}{I}\right|, \tag{6}$$

where I is the applied current and $U(\mathbf{r}_1,\mathbf{r}_2)$ is the voltage between the points $\mathbf{r}_1$ and $\mathbf{r}_2$. For EMR devices such as that depicted in Fig. 1, we will consider voltage probes along one side of the semiconductor, as this is the probe configuration reported in the experiments.[2,6] In addition to the potentials, by means of the FEM we also obtain the magnetic-field-dependent current distribution. For the device displayed in Fig. 1, the current distribution is shown in Fig. 2. Here, we have used the parameters of the device type A as displayed in Table I. Since the contact resistance ρ_c between metal and semiconductor has not been specified, we took $\rho_c=0$. One observes that for vanishing magnetic field, the current flows straight from the current lead into the metal film, i.e., the length of the current path in the semiconductor is minimized. This is due to the fact that the resistivity of the metal is lower than that of the semiconductor. For increasing magnetic field, the current paths become more and more bent to the left-hand side of the setup in Fig. 2. This deflection is due to the Lorentz force. However, the shape of the current paths is also determined by the device geometry and the boundary conditions at the interface. The current density thus peaks near the left edge of the semiconductor-metal interface for higher magnetic fields. Such ''hot spots'' necessitated a refined mesh in the proximity of the interface edges as shown in Fig. 1. In the region around the right-hand edge of the interface the current density is diminished. For a higher magnetic field of a few teslas, our model predicts that the current peaks vanish, since in that case nearly all current flows within the semiconductor and barely enters the metal.

The resistance R, as defined in Eq. (6) and evaluated for different probe pairs, is shown in Fig. 3. For a symmetric probe configuration, the $R(B)$ curve is symmetric, while for an asymmetric probe configuration, the curve shows an asymmetry. This is in agreement with the behavior reported by Zhou *et al.*[2] In the following, we will focus on a symmetric probe configuration. In the inset of Fig. 3, we show the very good quantitative agreement between measurement and our FEM results. The FEM analysis is found to be a powerful technique to interpret the magnetoresistance data of EMR devices.

IV. MAGNETORESISTANCE OF A 2DES-METAL HYBRID STRUCTURE

The application of the two-dimensional model described in Sec. III to a real structure usually requires the existence of a translation symmetry of the three-dimensional device along the z direction, since only then can Eq. (5) be separated into an x-y, and a z contribution. This is, e.g., the case for bulk

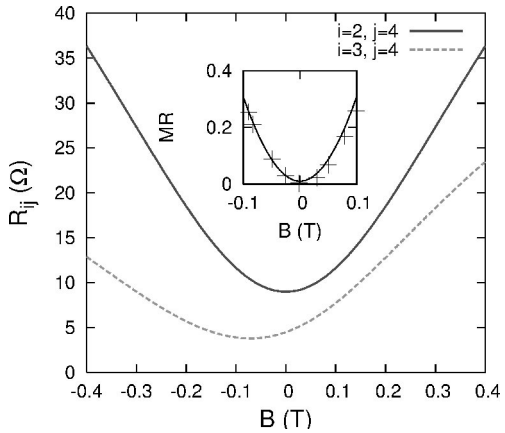

FIG. 3. $R(B)$ curves for different pairs of voltage probes labeled by i and j. The geometry and the placement of the current leads are those of Fig. 1. The device dimensions and material parameters are those of type A in Table I. The inset shows the magnetoresistance (MR) in a symmetric probe configuration (2,4) obtained by the FEM compared with the experimental data of Zhou *et al.*[2]

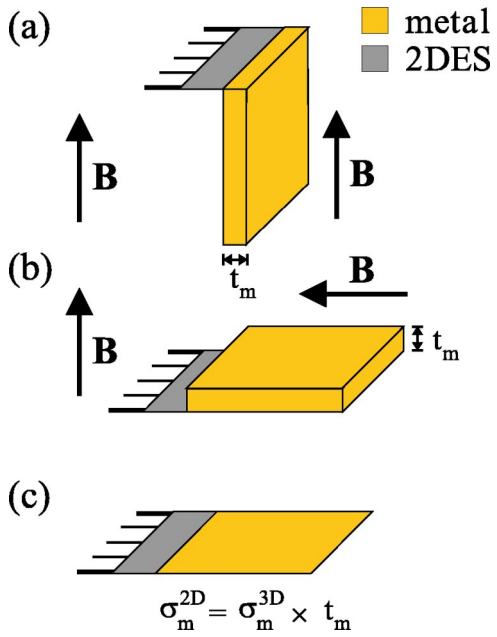

FIG. 4. Two-dimensional model for a hybrid structure, where a 2DES is in contact with a 3D metal (a). The modeling procedure consists first of a virtual rotation of the metal film along the 2DES-metal interface axis, so that it lies in the same plane as the 2DES (b). The three-dimensional film is compressed to a two-dimensional metal film of conductivity σ_m^{2D} (c). The contacts are schematically drawn on the left-hand side of the device.

semiconductor-metal hybrid structures analyzed in Sec. III. EMR devices consisting of a 2DES-metal hybrid structure as investigated by Möller *et al.*[6] and by Solin *et al.*[4] and as drafted in Fig. 4(a) lack this symmetry. Creating a three-dimensional mesh suitable for a detailed FEM analysis of these structures would require more than 10^9 nodes, which imposes an enormous challenge on the simulation software. For this reason, we will develop a two-dimensional model of the 2DES-metal hybrid structures. Our approach is outlined in Fig. 4. Here, we make use of the fact that the current distribution is homogeneous in the thickness t_m of the metal film, which for the device studied in Ref. 6 was 500 nm. It varies mainly in the direction parallel to the B field in Fig. 4(a). The width of the metal film in this direction was 500 μm in Ref. 6.

First, we rotate the metal film by 90^0 along the 2DES-metal interface axis, such that both components lie in the same x-y plane as depicted in Fig. 4(b). This rotation, in general, means that also the magnetic field which acts on the metal is rotated along the same axis. The mobility of electrons in a metal is typically very low such that the dimensionless parameter β [Eq. (3)] in the metal is effectively zero in the magnetic-field regime discussed in this work. In a second step, we compress the metal to a two-dimensional film as shown in Fig. 4(c). The two-dimensional conductivity of such a metal film σ_m^{2D} is recalculated from the three-dimensional conductivity σ_m^{3D} by

$$\sigma_m^{2D} = \sigma_m^{3D} \times t_m , \tag{7}$$

where t_m is the original thickness of the metal. Equation (7) is assumed to be valid as long as t_m is small and the current flows through the entire thickness of the metal film. The relevant data for the two-dimensional analysis are given by the electron density $N_s(1/\mathrm{m}^2)$ in the 2DES, the mobility μ (1/T), and the metal conductivity σ_m^{2D} $(1/\Omega)$. The zero-field conductivity of the 2DES is then

$$\sigma_0 = N_s e \mu \tag{8}$$

and its physical dimension is also $(1/\Omega)$. This model for 2DES-metal hybrid structures allows an application of the FEM as described in Sec. II.

In this paper, we do not discuss the quantum phenomena occurring in a 2DES-metal hybrid structure at low temperatures and high magnetic fields. These are, e.g., Shubnikov-de-Haas oscillations as observed in Refs. 6, 7. In the low magnetic-field regime, where the EMR effect is observed, the magnetoresistance can be modeled by Eqs. (2) and (4).

V. EFFECT OF CONTACT RESISTANCE

Modeling of EMR devices[2,9] has so far not considered the contact resistance at the semiconductor-metal interface. However, it has been observed very recently in experiments on microstructured hybrid devices that the contact resistance plays a decisive role.[8] In a mesoscopic device limit, a lower limit for the contact resistance can be recalculated from the Sharvin conductance[11] at zero magnetic field

$$G_M = \frac{2e^2}{h} M , \tag{9}$$

where M denotes the number of electron modes fitting through the contact area. Here, ballistic transmission through the contact area is assumed with a transmission coefficient of one. Considering a 2DES-metal hybrid structure as shown in Fig. 4, the Sharvin resistance is given by

$$R_{\mathrm{Sh}}^{2D} = \frac{h}{2e^2} \frac{\pi}{k_F a_c} , \tag{10}$$

where $k_F = \sqrt{2\pi N_s}$ is the Fermi wave number and a_c is the width of the 2DES-metal interface. We note that a real 2DES exhibits a finite thickness. We assume in the following that the relevant parameter for this extension in the z direction is the thickness t_c of the InAs quantum well, which is in contact with the metal. The specific contact resistance ρ_c can hence be obtained from Eq. (10) by

$$\rho_c^{\mathrm{Sh}} = R_{Sh}^{2D} \times a_c \times t_c . \tag{11}$$

For the values $a_c = 200$ μm and $t_c = 4$ nm from Ref. 6, we find $\rho_c^{\mathrm{Sh}} = 8.5 \times 10^{-9}$ $\Omega\,\mathrm{cm}^2$. We assume that this value represents the lower limit for such a 2DES-metal hybrid structure. Please note that ρ_c^{Sh} is a specific value for the given structure and is no longer dependent on, e.g., the geometrical parameter a_c.

In our model, we implement a magnetic-field-independent contact resistance between the semiconductor and the metal by inserting a contact layer of width b_{sc} as shown in Fig. 5.

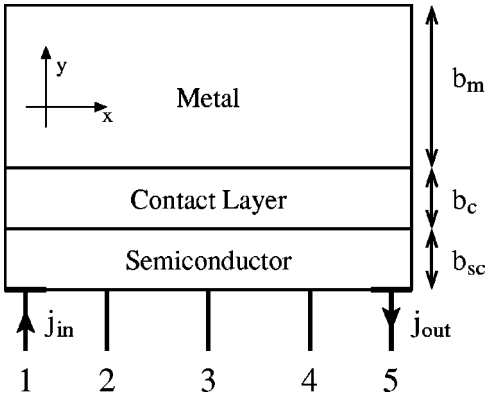

FIG. 5. Schematic drawing of the simulation setup, including an additional contact layer between semiconductor and metal, which will be used to model the interface resistance between both materials. The width of the semiconductor, of the contact region and of the metal are labeled by b_{sc}, b_c, and b_m, respectively.

This contact layer is characterized by a conductivity tensor, which does not depend on B and in x,y coordinates takes the form

$$\boldsymbol{\sigma}_c = \begin{pmatrix} 0 & 0 \\ 0 & \sigma_c \end{pmatrix}, \tag{12}$$

ensuring that the current flows in y direction through the contact region and has no x component within this region. The dimension of σ_c is $(1/\Omega)$.

In order to simulate a specific contact resistance ρ_c, we therefore choose a combination of the parameters b_c and σ_c, such that

$$\rho_c = \frac{b_c t_c}{\sigma_c}. \tag{13}$$

For reasons of numerical efficiency, we keep b_c fixed and, in order to simulate different values of ρ_c, vary σ_c. The value of b_c is chosen for purposes of the mesh generation. For simulating the device described by Möller *et al.*,[6] we, e.g., chose $b_c = 10\ \mu$m. Figure 6 shows the effect of different contact resistances on $R(B)$ curves for the type-B configuration in Table I. In the same figure, we compare our calculations to the experimental data obtained by Möller *et al.*[6]

We find by our calculations that a large value of the contact resistance keeps the current from entering the metal. At low magnetic field, the minimum value of $R(B)$ at $B=0$ T increases for higher ρ_c. In high magnetic field, the effect of the interface resistance on $R(B)$ becomes negligible, since the current flow is bent in the semiconductor and does not cross the interface, so that the asymptotic behavior of $R(B)$ is independent of ρ_c.

We find the best fit between FEM results and experimental data for a simulated contact resistance of $\rho_c^{\mathrm{FEM}} = 3.3 \times 10^{-8}\ \Omega\ \mathrm{cm}^2$. This value is only a factor of 2 larger than ρ_c extracted from experimental data.[8,12] The small deviation can be understood, since the contact resistance is the only adjustable parameter in our model, and hence captures all deviations between the FEM model and the real device, i.e., also those which do not originate from the contact resistance. We have also not included that the contact resistance might show a field dependence. The fact that, both, the experimentally determined value of ρ_c at $B=0$ and the simulated contact resistance are so close, shows the good agreement of FEM results and experimental data. A more detailed analysis of the experimental curves will be given elsewhere.[12] We concentrate here on general conclusions that can be drawn from our model and on theoretical predictions about the EMR effect.

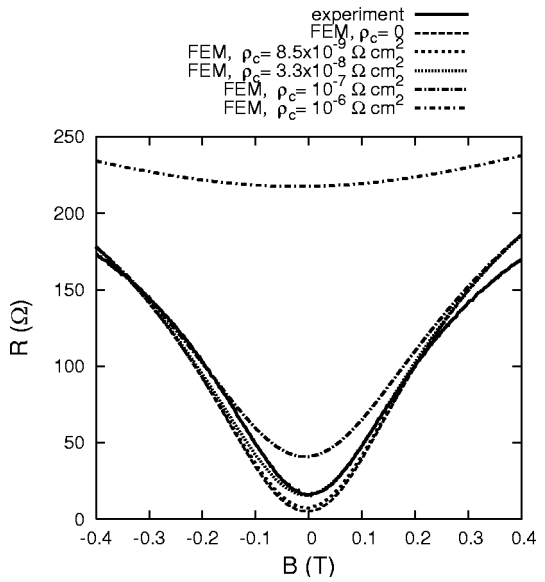

FIG. 6. $R(B)$ curves for the type-B device configuration from Table I. The experimental result (solid line) is compared to the results of the FEM analysis including a contact resistance of $\rho_c = \rho_c^{\mathrm{Sh}} = 8.5 \times 10^{-9}\ \Omega\ \mathrm{cm}^2$, $\rho_c = 3.3 \times 10^{-8}\ \Omega\ \mathrm{cm}^2$ (best fit to the experimental curve at $B=0$ T), $\rho_c = 1 \times 10^{-7}\ \Omega\ \mathrm{cm}^2$ and $\rho_c = 1 \times 10^{-6}\ \Omega\ \mathrm{cm}^2$. We also show the results for $\rho_c = 0$, which was assumed in earlier model calculations on the EMR effect.[2,9]

As shown in Fig. 7, varying the value of the contact resistance leads to different values for dR/dB and $1/R\ dR/dB$. We find the existence of a critical value of ρ_c, which is about $\rho_c^{\mathrm{crit}} = 10^{-6}\ \Omega\ \mathrm{cm}^2$ for the device modeled in Fig. 7. For values of ρ_c below ρ_c^{crit}, the magnetoresistance depends drastically on the exact value of ρ_c. At $\rho_c \approx \rho_c^{\mathrm{crit}}$, the current sensitivity rapidly decreases to zero in Fig. 7(b). In Fig. 7(c), the voltage sensitivity is already zero for ρ_c^{crit}. For values $\rho_c \gg \rho_c^{\mathrm{crit}}$, the magnetoresistance in Fig. 7(a) is independent of ρ_c. In this situation, the large ρ_c blocks the current from flowing across the interface, i.e., the charge transport is restricted to the 2DES. As a result, the resistance remains nearly unchanged when a magnetic field is applied. The voltage and current sensitivities are zero and the EMR effect is destroyed. For technological applications of the EMR effect, the control of ρ_c is hence a prerequisite.

From our FEM analysis, we find that ρ_c^{crit} depends on the width b_{sc} of the semiconductor. This is shown in Fig. 8, where the dependence of the current sensitivity on ρ_c at $B = 25$ mT is depicted for a modified type-B device configu-

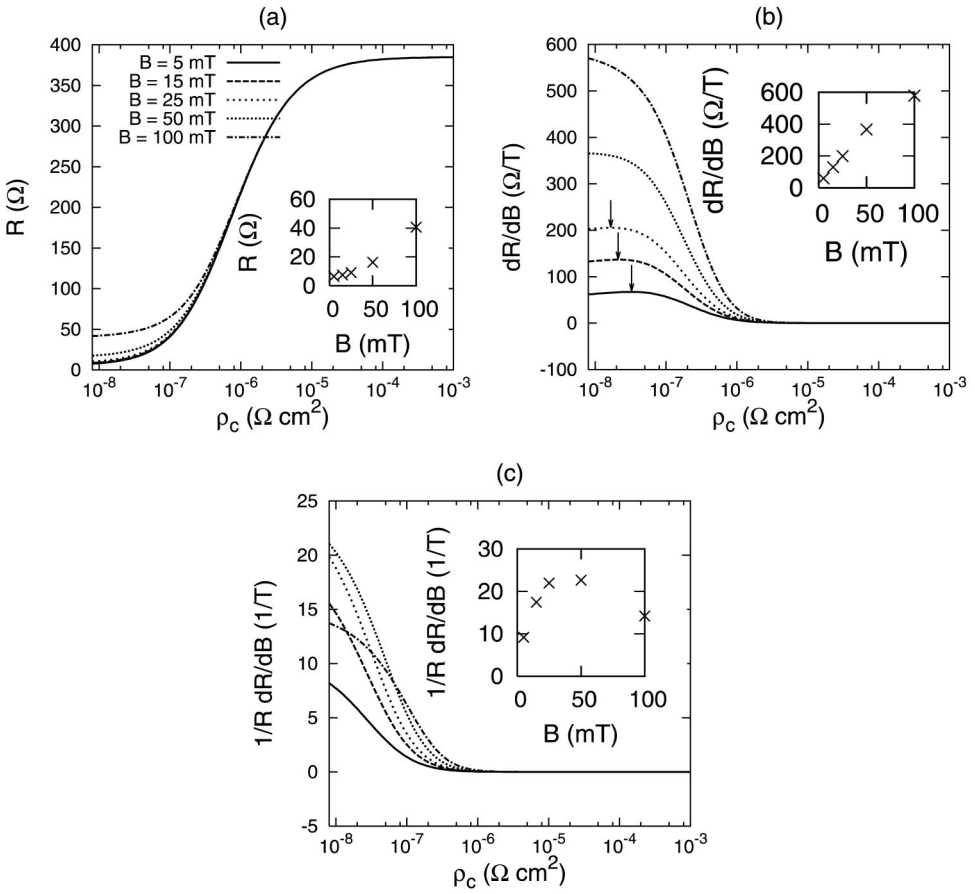

FIG. 7. The effect of contact resistance on (a) $R(B)$, (b) dR/dB, and (c) $1/R\ dR/dB$ at various values of the magnetic field. We refer here to the type-B device configuration of Table I for the 2DES-metal hybrid structure. The arrows in (b) point to the maximum values of dR/dB for a given magnetic field. The insets show the magnetic-field dependence of R, dR/dB, and $1/R\ dR/dB$, respectively, for $\rho_c = \rho_c^{\mathrm{Sh}}$.

ration with $b_{sc} = 7\ \mu$m. For comparison, the curve from Fig. 7(b) with $b_{sc} = 20\ \mu$m is included in the figure. We find that ρ_c^{crit} increases if b_{sc} decreases. In the regime where the device sensitivity depends on ρ_c, i.e., for $\rho_c \leqslant \rho_c^{\mathrm{crit}}$, interestingly, we observe local maxima of dR/dB [cf. arrows in Fig. 7(b)]. These are not very distinct for $b_{sc} = 20\ \mu$m. For $b_{sc} = 7\ \mu$m, however, the maxima are very prominent (cf. Fig. 8). Additionally, the maxima are shifted to higher values of ρ_c. From Fig. 8, we also extract that a large contact resistance can be compensated for by a smaller semiconductor width, i.e., dR/dB of the device with $b_{sc} = 7\ \mu$m becomes larger than dR/dB of the device with $b_{sc} = 20\ \mu$m for $\rho_c \geqslant 2 \times 10^{-7}\ \Omega\ \mathrm{cm}^2$. Such a tendency was also found experimentally by Möller *et al.*[8] It can be explained by the fact that a smaller b_{sc} increases the absolute resistance of the semiconductor which is shunted by the metal film. At the same time, the path resistance perpendicular to the interface becomes smaller. That means that the metal acts as a shunt for even higher values of ρ_c.

The insets in Fig. 7 show the magnetic-field dependence of the calculated device performance for $\rho_c = \rho_c^{\mathrm{Sh}}$, i.e., for the lower limit of the contact resistance. Here, we find that the current sensitivity dR/dB reaches large values at a higher magnetic field than the voltage sensitivity $1/R dR/dB$.

VI. EFFECT OF METAL CONDUCTIVITY

The EMR is not only affected by the quality of the semiconductor-metal interface alone, but also by the resistivity of the metal ρ_m. Most devices studied so far used gold or

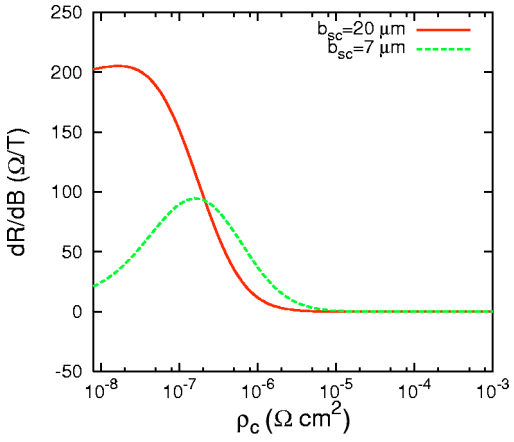

FIG. 8. The effect of contact resistance on dR/dB at $B = 25$ mT for a type-B device configuration with $b_{sc} = 20\ \mu$m and with a smaller width of $b_{sc} = 7\ \mu$m. The maximum of dR/dB occurs at a higher value of ρ_c, if we decrease the semiconductor width. Additionally, ρ_c^{crit} is larger for smaller b_{sc}.

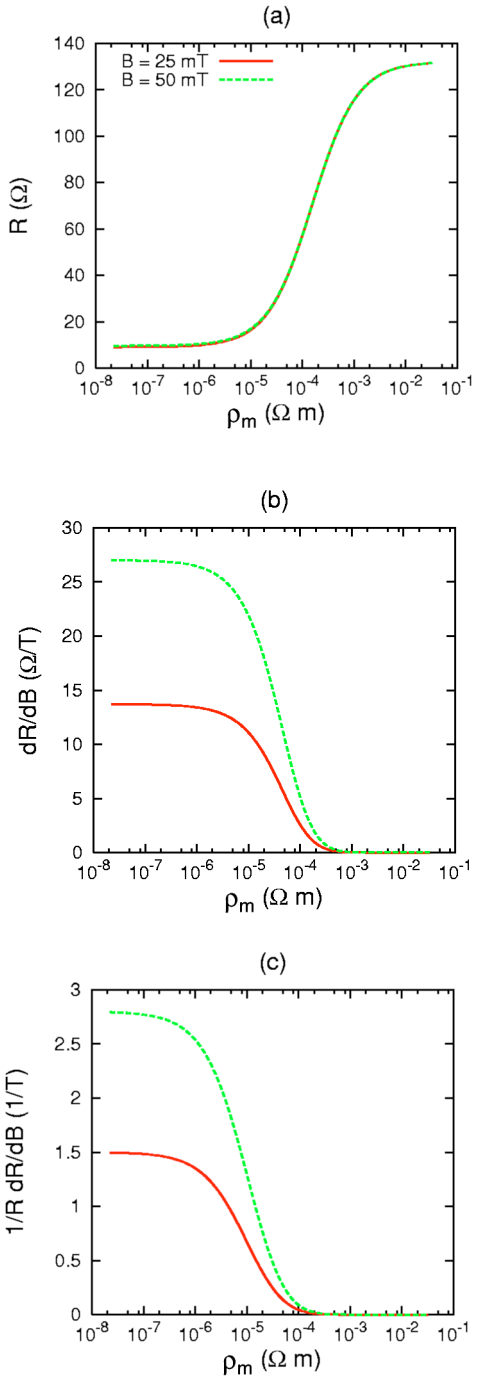

FIG. 9. The impact of the metal conductivity on (a) $R(B)$, (b) dR/dB, and (c) $1/R\,dR/dB$ at 25 mT and 50 mT for a type-A device configuration. Here, we have assumed $\rho_c=0$ in order to show the effect of ρ_m alone. ρ_m in Ref. 2 was 2.2×10^{-8} Ω m.

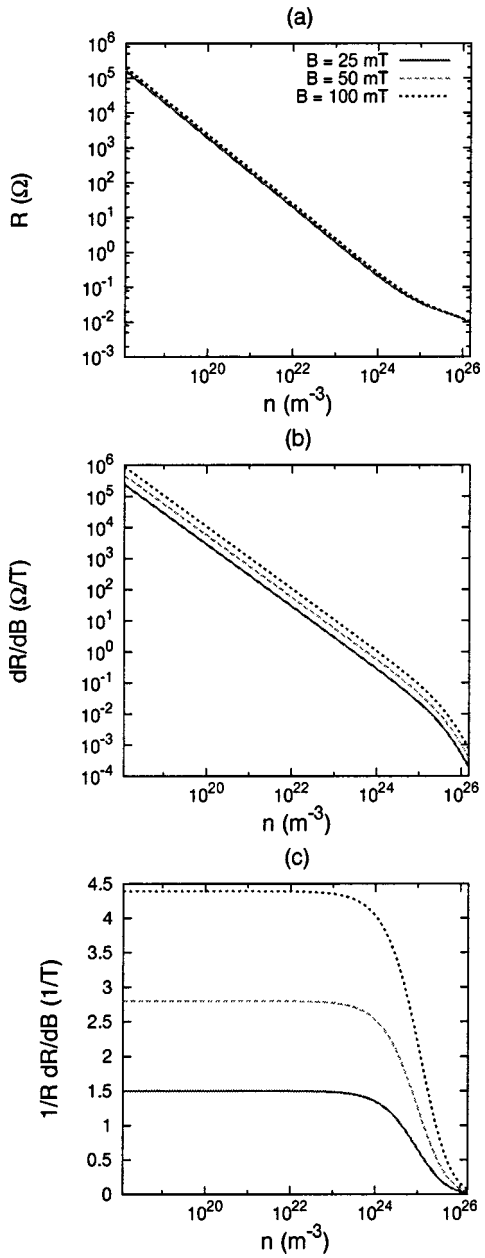

FIG. 10. The effect of variations of the carrier concentration on (a) R, (b) dR/dB, (c) $1/R\,dR/dB$ based on the type-A device configuration of Table I. At 7×10^{25} m^{-3}, the conductivity of the semiconductor equals that of the metal. For much higher values, the metal does not act as a shunt anymore.

an alloy with gold as a material for the shunt.[1,5,6] In our model calculation, we have varied the resistivity of the metal ρ_m and evaluated its effect on $R(B)$, dR/dB, and $1/RdR/dB$. This is shown in Fig. 9 for magnetic fields of 25 mT and 50 mT on the basis of the type-A device configuration of Table I. In Fig. 9 the EMR properties remain nearly unchanged up to $\rho_m=10^{-6}$ Ω m. For $\rho_m<10^{-6}$ Ω m, the resistivity of the metal is much lower than that of the semiconductor, so that an increased ρ_m does not significantly alter the overall resistance of the device. For resistivities higher than about 2×10^{-6} Ω m, the resistance R rapidly increases. Simultaneously, the current and voltage sensitivities decrease. At $\rho_m=7\times10^{-5}$ Ω m, the conductivity of the metal equals that of the semiconductor. A variation of ρ_m around this particular value has a significant impact on the overall resistance and on the device sensitivity. For values of the metal resistivity of more than 0.01 Ω m, the metal does no longer play the role of a shunt, since the conductivity of the semiconductor is then much higher than that of the metal. The current or voltage sensitivity of the hybrid structure in

that case is zero. As in the case of a large ρ_c, the current flows mainly inside the semiconductor region and its distribution is not significantly changed by applying a magnetic field.

Our results are important as they show that using a less conductive or less pure (and thereby perhaps less expensive) metal does not significantly deteriorate the EMR behavior of the hybrid structure which was presented in Ref. 2. Here, the authors used a gold shunt with $\rho_c = 2.2 \times 10^{-8}\ \Omega\,\mathrm{m}$. In their case, ρ_m might even be a factor of 100 larger without degrading the device sensitivity.

It is important to notice here that by virtue of the two-dimensional FEM model for 2DES-metal hybrid structures described in Fig. 4, these considerations also apply to variations of the thickness of the metal film t_m, since here the product of film thickness and conductivity enters the model calculations via σ_m^{2D} [Eq. (7)].

VII. EFFECT OF CARRIER CONCENTRATION AND MOBILITY

The carrier concentration n of the three-dimensional bulk semiconductor, or N_s of the 2DES, enters the FEM analysis via the conductivity in zero magnetic field σ_0 as expressed in Eq. (4). The mobility μ enters in, both, σ_0 [Eq. (4)] and $\beta = \mu B$ [Eq. (2)]. In our model, we can vary the carrier concentration and the mobility separately. In practice, this might be difficult for bulk samples, however, for modulation-doped heterostructures, both, N_s and μ can be varied nearly independently over large regimes.

The dependence of R, dR/dB, and $1/R\ dR/dB$ on carrier concentration for a type-A device is shown in Fig. 10. Increasing the carrier concentration leads to a larger conductivity of the semiconductor and thereby to a lower value of the device resistance. For a concentration of $n_{\mathrm{crit}} = 7 \times 10^{25}\ \mathrm{m}^{-3}$, the conductivity of the semiconductor equals that of the metal. At concentrations higher than that, the metal is no longer effective as a shunt and the EMR effect degrades. For values of n which are much smaller than $7 \times 10^{25}\ \mathrm{m}^{-3}$, both the resistance and the current sensitivity lie on a straight line when displayed in the double-logarithmic plot of Fig. 10. From the slope of these curves, a $1/n$ behavior of, both, $R(n)$ and $dR/dB(n)$ is obtained for a fixed field B. This behavior is also expected from Eq. (4). Accordingly, the voltage sensitivity $1/R\ dR/dB$ remains constant over a broad regime of the carrier density. For a technical application, the carrier density should therefore be kept well below n_{crit}. However, the concrete value of n does not play a significant role for $1/R\ dR/dB$. By setting the parameter n, it is thus possible to adjust the resistance of the hybrid structure to some desired value for a certain magnetic field without affecting the voltage sensitivity. Only the current sensitivity will change accordingly. The value n_{crit} depends on the mobilityμ in the semiconductor. The effect of the latter parameter will be discussed in the following.

The impact of the carrier mobility μ in the semiconductor on the EMR effect is more complex. In the following, we keep the carrier concentration constant for the analysis. The shape of the $R(B)$ curves for different mobilities is depicted in Fig. 11 for a type-A device configuration. The impact of an increased mobility on these curves can be described by two effects.

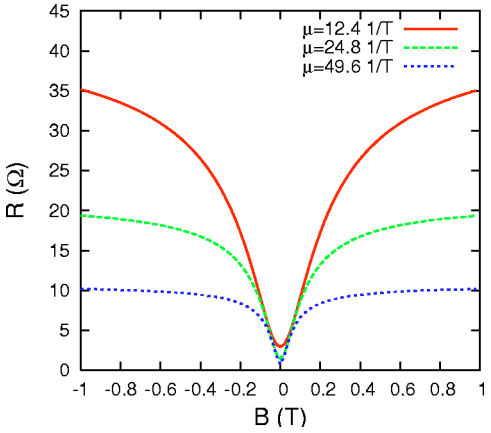

FIG. 11. The variation of the carrier mobility in the semiconductor leads to different $R(B)$ curves. The calculations are based on a configuration of type A in Table I. One observes that the magnetic-field interval with finite values of the current sensitivity increases for lower mobilities.

First, the zero-field resistance decreases, as it is mainly determined by σ_0, as long as the metal resistivity can be neglected. According to Eq. (4) the dependence of $R(B = 0\ T)$ on μ should then be almost reciprocal. The resistance at very high magnetic fields should also show a $1/\mu$ behavior, since then effectively no current enters the metal and the resistance is solely determined by the properties of the semiconductor. If this was the only effect, $R(B)$ would scale with μ for all magnetic fields in the same manner as with the carrier concentration n.

However, second, a variation of μ changes the device performance considerably also for intermediate magnetic fields. The field, where $R(B)$ levels off moves to a higher value B, i.e., the operation region of the device is enlarged for smaller values of μ. The effect of μ is in this respect similar to a scaling factor along the B axis.

In the following, we analyze the effect of μ in more detail. One finds a distinct maximum of the current sensitivity dR/dB and the voltage sensitivity $1/R\ dR/dB$ for each of the three magnetic fields displayed in Fig. 12. This means that for an optimization of an EMR device as a magnetic-field sensor at a specific value of the magnetic field B, one should utilize a semiconductor exhibiting a certain value of the mobility. The value of $1/\mu$ for which $dR/dB(\mu,B)$ has a maximum for a fixed magnetic field B depends linearly on B, as shown in Fig. 13. This can be explained by the dependence of R on the dimensionless field β. Once a value β is found, for which the current sensitivity becomes maximal, it remains maximal for different values of B as long as the product $\beta = \mu B$ is unchanged. For the type-A configuration the maximum is determined by $\mu B = 0.8$, which can be derived from the slope of the curve displayed in Fig. 13. Optimizing the current sensitivity for a higher magnetic field thus requires a lower mobility. The maxima of $dR/dB(\mu)$ for the type-A configuration take the same value of 90 Ω/T for all

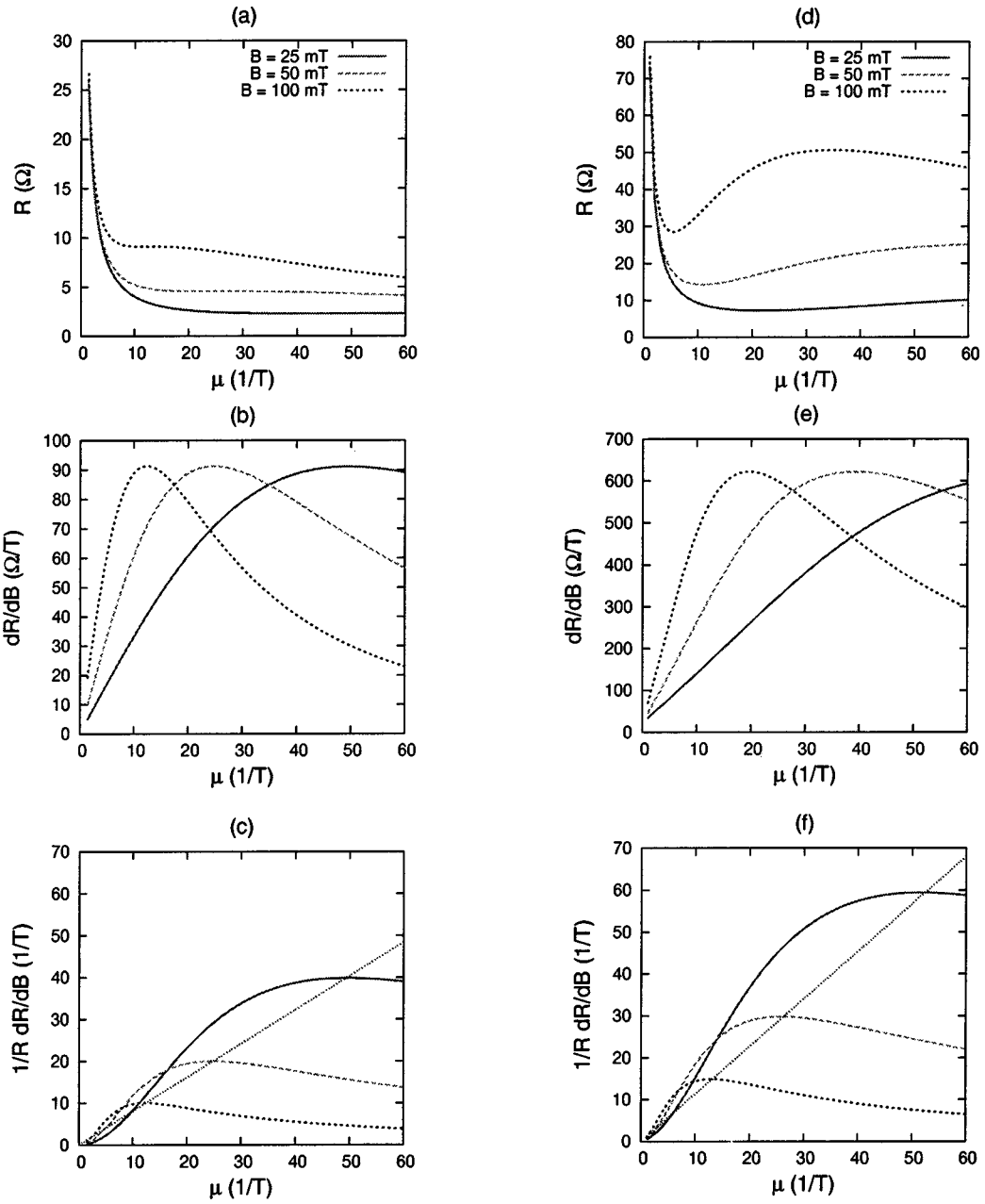

FIG. 12. The effect of varying the carrier mobility in the semiconductor on (a) $R(B)$, (b) dR/dB, and (c) $1/R dR/dB$ at 25 mT, 50 mT, and 100 mT for a type-*A* device configuration (Table I). On the right-hand side, labeled from (d) to (f), data for the type-*B* device configuration are plotted. In (c) and (f) the maxima of the curves are connected with a straight line. On the *x* axis, we depict the regime of mobilities which have been achieved in InAs-based quantum-well structures in low-temperature experiments.

three magnetic fields displayed in Fig. 12(b). This value depends on the device geometry. Varying the carrier concentration leads to different maximum values of dR/dB, but, both, the values μ, for which these maxima occur, and $1/R\, dR/dB$ remain unchanged. The maxima of $1/R\, dR/dB(\mu)$ for the type-*A* device configuration are found to lie on a straight line with the same slope of 0.8 and passing through the origin. In Figs. 12(d)–12(f), the corresponding results for the type-*B* configuration are shown. In Fig. 12(e) we find a maximum of dR/dB of about 600 Ω/T. One observes that the maxima of $1/R\, dR/dB(\mu)$ now lie on a straight line with a different slope of 1.1. Again, this slope is independent of the carrier concentration over a broad regime, but is found to be affected by the device geometry.

VIII. SUMMARY AND DISCUSSION

We have applied the FEM to, both, macroscopic hybrid structures with lateral dimensions on the millimeter scale and mesoscopic samples with lateral dimensions on the micrometer scale and studied their magnetoresistance behavior. We have shown that the finite element method is a versatile tool in analyzing and predicting the properties of EMR devices.

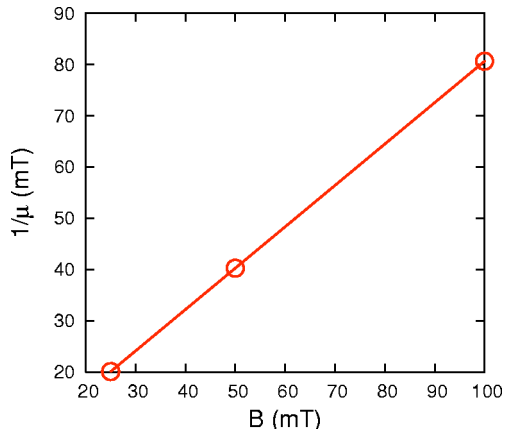

FIG. 13. The values of $1/\mu$, for which $dR/dB(\mu,B)$ becomes maximal as a function of B for the type-A device configuration. The calculated points lie on a straight line passing through the origin.

By means of FEM, it is possible to study systematically the influence of the material parameters on the magnetoresistance before physically fabricating the devices. It thus allows design studies and optimization of devices for specialized sensor applications. In particular, we found that an increased contact resistance can deteriorate the device performance. To some extent this can be compensated for by miniaturising the hybrid structure.

ACKNOWLEDGMENTS

We gratefully acknowledge continuous support of the work by D. Heitmann, stimulating discussions with D. Pfannkuche and experimental support by C. H. Möller. We thank the Deutsche Forschungsgemeinschaft for financial support via SFB 508 and the BMBF via Grant No. 01BM905.

-

*Electronic address: mholz@physnet.uni-hamburg.de

[1] S.A. Solin, T. Thio, D.R. Hines, and J.J. Heremans, Science **289**, 1530 (2000).
[2] T. Zhou, D.R. Hines, and S.A. Solin, Appl. Phys. Lett. **78**, 667 (2001).
[3] T. Zhou, S.A. Solin, and D.R. Hines, J. Magn. Magn. Mater. **226–230**, 1976 (2001).
[4] S. Solin, D.R. Hines, A.C.H. Rowe, J.S. Tsai, Y.A. Pashkin, S.J. Chung, N. Goel, and M.B. Santos, Appl. Phys. Lett. **80**, 4012 (2002).
[5] S.A. Solin, D.R. Hines, J.S. Tsai, Y.A. Pashkin, S.J. Chung, N. Goel, and M.B. Santos, IEEE Trans. Magn. **38**, 89 (2002).
[6] C.H. Möller, O. Kronenwerth, D. Grundler, W. Hansen, Ch. Heyn, and D. Heitmann, Appl. Phys. Lett. **80**, 3988 (2002).
[7] O. Kronenwerth, C. H. Möller, D. Grundler, Ch. Heyn, and D. Heitmann, in *Toward the Controllable Quantum States*, edited by Hideaki Takayanagi and Junsaku Nitta (World Scientific, Singapore, 2003), p. 99.
[8] C. H. Möller, D. Grundler, O. Kronenwerth, Ch. Heyn, and D. Heitmann, JOSC **16**, 195 (2003).
[9] J. Moussa, L.R. Ram-Mohan, J. Sullivan, T. Zhou, D.R. Hines, and S.A. Solin, Phys. Rev. B **64**, 184410 (2001).
[10] B. Niceno, EasyMesh (Division of Applied Physics, University of Trieste, Italy, 1996), Mesh Generator downloadable from http://www-dinma.univ.trieste.it/~nirftc/research/easymesh/
[11] Y.V. Sharvin, Sov. Phys. JETP **21**, 655 (1965).
[12] O. Kronenwerth, M. Holz, C. H. Möller, D. Grundler, Ch. Heyn, and D. Heitmann (unpublished).